The role of Rossby wave breaking in shaping the equilibrium atmospheric circulation response to North Atlantic boundary forcing

Courtenay Strong *

University of California, Irvine

Gudrun Magnusdottir

University of California, Irvine

March 25, 2009

* *Corresponding author address:* Courtenay Strong, Department of Earth System Science, University of California Irvine, Irvine, CA 92697.

E-mail: cstrong@uci.edu

ABSTRACT

Rossby wave breaking (RWB) is shown to play a central role in the transient response of an atmospheric global climate model to boundary forcing by sea ice anomalies related to the North Atlantic Oscillation (NAO). When the NCAR Community Climate Model 3 was forced by an exaggerated sea ice extent anomaly corresponding to one arising from a positive NAO, a localized baroclinic response developed and evolved into a larger-scale equivalent barotropic pattern resembling the negative polarity of the NAO. The initial baroclinic response shifted the phase speeds of the dominant eddies away from a critical value equal to the background zonal flow speed, resulting in significant changes in the spatial distribution of RWB. The forcing of the background zonal flow by the changes in RWB accounts for 88% of the temporal pattern of the response, and 80% of the spatial pattern of the zonally averaged response. Although results here focus on one experiment, this "RWB critical line mechanism" appears relevant to understanding the equilibrium response in a broad class of boundary forcing experiments given increasingly clear connections among the northern annular mode, jet latitude shifts, and RWB.

1. Introduction

The response of atmospheric general circulation models to boundary forcing is quite varied across models and experiments (Kushnir et al. 2002), and has been challenging to interpret because of nonlinearities with respect to the sign of the forcing anomaly (Kushnir and Lau 1992; Peng et al. 2002, 2003; Ferreira and Frankignoul 2005), and the location of the forcing anomaly relative to the storm track (Peng et al. 1997). Despite these complexities,

studies of transient eddy feedback have provided some clues as to the physical processes underlying these varied response patterns, particularly when the response projects onto the northern annular mode (NAM) or North Atlantic Oscillation (NAO). In such cases, it has been suggested that the response is in balance with patterns of eddy vorticity flux divergence (e.g., Robinson 2000; Kushnir et al. 2002; Peng et al. 2003).

The purpose of the present paper is to illustrate the role of Rossby wave breaking (RWB) in the time evolution of the atmospheric response to boundary forcing, where RWB refers to the rapid, irreversible overturning of potential vorticity (PV) on isentropic surfaces (McIntyre and Palmer 1983). By explicitly examining how RWB contributes to the development of NAO-like response patterns, we aim to add dynamic specificity to the "transient eddy feedback" to which such response patterns are often attributed. Although we anticipate that RWB is relevant to a broad class of boundary forcing experiments, we base the presentation here on a particular set of experiments with one type of forcing that was conducted with the NCAR Community Climate Model 3 (CCM3).

Specifically, Magnusdottir et al. (2004) and Deser et al. (2004) found a strong, winter mean response when forcing CCM3 with sea-ice extent anomalies corresponding to a strong positive NAO. In a recent paper, Deser et al. (2007, hereinafter referred to as DTP) extended this study by considering daily output from a large ensemble of experiments forced in the same way, each extending from November through April. They documented the daily evolution of the response from an initial baroclinic response, restricted in horizontal extent to the area of the forcing and nearby regions, to an equivalent barotropic response that is hemispheric in scale. DTP further showed, using a linear baroclinic model, that the equilibrium response is maintained by nonlinear transient eddy fluxes, but they did not suggest a

physical mechanism bridging the initial baroclinic, horizontally restricted response and the subsequent, large-scale equivalent barotropic response.

Here, we present evidence that RWB is the bridging mechanism that shapes the equilibrium response in the ICE experiment [1]. Since the equilibrium response is NAO-like, the idea that RWB is important follows logically from previous studies establishing the role of RWB, or RWB proxies such as eddy momentum flux, in maintaining NAO-like variability (Franzke et al. 2004; Abatzolglou and Magnusdottir 2006; Riviere and Orlanski 2007; Strong and Magnusdottir 2008). Since polarity changes of the NAO are associated with shifts in the latitude of the eddy-driven jet, our results are also related to recent research connecting jet shifts to changes in the phase speed of dominant eddies or the background zonal flow (Chen et al. 2007; Chen and Zurita-Gotor 2008).

Analyzing the output of the ICE experiment in the context of RWB, we find that 1) the initial, baroclinic response shifts dominant eddy phase speeds so as to alter the spatial distribution of Rossby wave breaking, and 2) the changes in RWB relative frequency force the background zonal flow in a manner accounting for more than 80% of the temporal and spatial patterns of the response. We present methods in Section 2, followed by two results sections describing RWB variability driven by the ICE forcing (Section 3a) and its effect on the atmospheric response (Section 3b).

[1]The ICE experiment examined here was forced by the same sea ice extent as the ICE2 experiment in Magnusdottir et al. (2004).

2. Methods

a. Model output

We analyze the same experiments as in DTP. For the ICE case, the sea-ice areal extent forcing varied slightly through the season, but the mid-January anomalies in Fig. 1a are representative (complete details on the model configuration and forcing are given in DTP). Briefly, a 240-member ensemble of integrations was developed by forcing CCM3 (T42 with 18 vertical levels) with the ICE anomaly pattern, with each member running from 1 December to 30 April with unique initial conditions taken from a long, unforced run. To provide a control, a second 240-member ensemble of integrations was developed using the same series of initial conditions as the ICE experiment, but with climatological sea-ice extent.

For each of the 240 members, the forced and unforced runs provide a pair of integrations with the same initial conditions. The response to the forcing on a particular day of the experiment is obtained by subtracting each control result from its paired anomaly experiment for that day and then averaging across all the ensemble members for that day. This response is a function of space and time, is denoted by a prefix δ, and may have a subscript to indicate that it has been averaged over specific days of the integration. For example, δu_{1-14} is the zonal wind response averaged over the first fourteen days of the experiment and has values at each grid point over the hemisphere.

b. RWB analysis

For the control and forced ensembles, we calculated PV on the 350-K isentropic surface using daily average [2] fields of pressure, temperature, and horizontal velocity $\mathbf{v} \equiv (u, v)$. We then identified all instances of anticyclonic RWB for the Northern Hemisphere following the method detailed in Strong and Magnusdottir (2008), hereafter SM8. Using Fig. 2 to briefly describe the method, we identify regions where circumpolar PV contours are overturned anticyclonically (Fig. 2a) or cyclonically (Fig. 2b). We then measure the area of the poleward tongue of the overturning contour (shaded regions, Figs. 2a,b), and record the longitude-latitude (λ, ϕ) coordinates of the poleward tongue's centroid (filled circles, Fig. 2a,b). We then quantify how often anticyclonic or cyclonic RWB centroids are observed within $N = 400$ equal-area bins over the Northern Hemisphere. For each bin centered on $(\lambda, \phi)_n, n = 1, 2, \ldots, N$, we calculate the relative frequency of anticyclonic RWB centroids, which is a dimensionless quantity given by

$$\gamma_a(\lambda, \phi)_n \equiv \frac{1}{\tau} \sum_{t=1}^{\tau} \beta((\lambda, \phi)_n, t) \tag{1}$$

where τ is the number of daily observations in the period for which γ is calculated, and the event parameter β takes the value 1 when an anticyclonic centroid is located in the bin at time t and zero otherwise. A corresponding variable for cyclonic RWB denoted by γ_c is also calculated. We refer to regions of frequent RWB as "surf zones," defined by the threshold $\gamma_a, \gamma_c \geq 0.04$. The surf zones in the CCM3 simulations (not shown) correspond well with the observational surf zones shown in Fig. 2 of SM8.

[2] It would be preferable to use instantaneous twelve- or six-hourly output for these calculations, but the experimental design only specified daily mean output.

c. Forcing of background flow by RWB

We calculated the composite forcing exerted on the background flow by anticyclonic and cyclonic RWB following the method used to generate Fig. 3 in SM8. Briefly, the forcing of the background zonal wind speed is given by the divergence of the vector $\boldsymbol{E} \equiv (\overline{v'^2 - u'^2}, -\overline{u'v'})$ (see appendix A in Hoskins et al. 1983), where a prime indicates deviation from an average taken for a particular day of year and location over all ensemble members. We randomly selected 200 cases of RWB from different regions in the model, aligned them at their centroids, calculated $\nabla \cdot \boldsymbol{E}$ for each regional set, and then zonally averaged the results from 30° west of the centroid to 30° east of the centroid. The results from the control and forced ensembles (not shown) closely resemble those in Figs. 3a and 3b of SM8, indicating that anticyclonic RWB tends to accelerate the zonal flow on its poleward flank and decelerate the zonal flow on its equatorward flank, whereas cyclonic RWB exerts the opposite forcing. We will refer to these fundamental composite $\nabla \cdot \boldsymbol{E}$ patterns as the the RWB $\bar{u}$-forcing patterns in section 3.

d. Statistics

To test the significance of the model's response to forcing, we compared the mean of the forced ensemble to the mean of the control ensemble using a t-test that accounts for serial and cross correlation in the samples (e.g., Wilks 1995, Chapter 5). To develop multiple linear regression models, we used a backward stepwise bootstrap regression based on the Akaike information criterion (AIC). Regressors were included in the model if they were retained in at least 60% of the 1000 resampled iterations – a procedure shown to produce parsimonious

models with excellent predictive capability (Austin and Tu 2004). An empirical orthogonal function (EOF) is the unit length spatial eigenvector of the area-weighted covariance matrix of a scalar field. The associated principal component time series is the standardized (zero mean, unit standard deviation) projection of the corresponding data onto the EOF.

3. Results

In the first results subsection (3a), we show that the initial baroclinic response is associated with changes in the background zonal flow and eddy phase speeds that lead to shifts in the relative frequency of RWB. In the second results subsection (3b), we show how these changes in RWB force the background zonal flow via eddy momentum flux convergence anomalies, accounting for more than 80% of the spatial and temporal patterns of the large-scale equivalent barotropic response.

a. Response in zonal wind and eddies

DTP describe the transient response in the ICE experiment in terms of geopotential height on the 1000, 650 and 300 hPa isobaric surfaces (their Fig. 6). We find it useful to supplement this view by examining the transient response in zonal wind (Fig. 3) and eddy phase speeds (Fig. 4). These two additional perspectives provide a useful supplementary view because RWB occurs near "critical lines" in the velocity field where the phase speed of incoming waves equals the background zonal wind speed (Randel and Held 1991), and RWB in turn feeds back onto the background zonal flow (SM8). The localized baroclinic

response that develops during days 1-14 (see DTP) is in approximately geostrophic balance with a zonal wind anomaly pattern on the 350-K surface with centers of action approximately aligned along 42°W (δu_{1-14}, Fig. 3a). The 350-K u response for the remainder of the experiment (δu_{15-151}, Fig. 3b) resembles the upper-tropospheric u anomaly pattern associated with the negative polarity of the NAO. Comparison of Figs. 3a and 3b from 42°W to 0° illustrates that the equivalent barotropic response can be thought of as a translation or extension of the initial baroclinic response downstream.

To examine the role of the model's dominant eddies in this downstream translation, we decomposed the transient eddy momentum flux at 350K into contributions from different zonal phase speeds as a function of latitude (Hayashi 1971) for the first two months of the experiment. The shading in Fig. 4a shows results averaged across the control ensemble. Similar to the observational results in Randel and Held (1991), the control eddy momentum flux was predominantly positive with a maximum near 35°N, indicating generally equatorward wave propagation from a midlatitude source region. The contours in Fig. 4a show the response in eddy momentum flux. The response involved a shift toward slower phase speeds around 55°N (contoured dipole, Fig. 4a). Further decomposing the spectrum in Fig. 4a by wave number following Randel and Held (1991), we see that the reduction in phase speed about 55° was associated with an increase in energy near wave number 4 and a decrease in energy near wave number 6 (Fig. 4b). The response also involved a shift toward higher phase speeds around 30°N (Fig. 4a) with a less pronounced shift in dominant wave number (not shown).

The shift toward lower phase speeds around 55°N in the forced experiment (contours, Fig. 4a) is toward the left on the phase axis, which is away from the critical line where

the background zonal wind and phase speed match (bold curve, Fig. 4a). This shift away from critical phase speeds would be consistent with a reduction in the relative frequency of RWB over these latitudes. Indeed, the relative frequency of anticyclonic RWB is substantially reduced near 55°N (γ_a response, Fig. 4c). The increase in phase speeds near 30°N is separated from, but still toward, the critical line (Fig. 4a) which would be consistent with the modest collocated increase in γ_a (Fig. 4c). Fig. 4c shows that smaller responses in cyclonic RWB also occurred. These γ_c anomalies made a non-negligible contribution to the total response as we will show in the next section. The decomposition of eddy momentum flux into phase speed / zonal wave number space appears less useful for elucidating the dynamics leading to the γ_c changes, in part because the method highlights dominant eddy processes. Rather than being dominant, the cyclonic response is more longitudinally confined as shown in section 3b, and the cyclonic surf zones over the Euro-Atlantic sector are approximately one third as active as the anticyclonic surf zones (not shown here, see Fig. 2 in SM8).

b. Role of RWB in the response

In this subsection, we show that changes in the relative frequency of RWB account for more than 80% of the spatial and temporal patterns of the response. Beginning with the spatial pattern, we use shading in Fig. 5 to show the principal regions of positive and negative zonal wind response from Fig. 3b, and superimpose the response patterns of RWB relative frequency ($\delta\gamma_a$ and $\delta\gamma_c$ contouring, Fig. 5). Approximately three quarters of the surface area bounded by $\delta\gamma$ contours in Fig. 5 have γ response anomalies that are significant at the 95% confidence level based on a t-test. The alignment of the zonally elongated δu_{15-151}

and $\delta\gamma$ response bands follows logically from how RWB forces the background zonal flow (the RWB $\bar{u}$-forcing patterns discussed in Section 2c), and the A1, A3, A5, and C5 regions identified in Fig. 5 correspond to RWB regions studied in detail in connection with the NAO in SM8. Consistent with the $\bar{u}$-forcing pattern of anticyclonic RWB, regions of positive $\delta\gamma_a$ (e.g., the A5 region in Fig. 5a) are flanked to the north by positive δu_{15-151} and to the south by negative δu_{15-151}. Regions of negative $\delta\gamma_a$ (e.g., the A3 and A1 regions in Fig. 5a) are flanked to the north by negative δu_{15-151} anomalies and to the south by positive δu_{15-151} anomalies, again consistent with the $\bar{u}$-forcing pattern of anticyclonic RWB.

Considering the $\bar{u}$-forcing pattern of cyclonic RWB, regions of positive $\delta\gamma_c$ such as C5 in Fig. 5b contribute to the δu_{15-151} response, which is positive to the south of C5 and negative to the north. The γ_c increase in C5 acts cooperatively with the γ_a reduction in A3 to generate the zonal wind response pattern. The reduction in γ_c over the high latitudes of North America, by contrast, is analogous to the C1 region discussed in SM8. Specifically, it acts in opposition to the γ_a reduction over the Pacific and North America, contributing to the disruption of zonal symmetry across these longitudes.

To further illustrate the latitudinal alignment of the response and the RWB anomalies, we modeled the zonally averaged zonal wind response using the RWB $\bar{u}$-forcing patterns from the A3, A5, and C5 regions (patterns defined in section 2c). In Fig. 6, the bold curve is the zonal average of the δu_{15-151} response in Fig. 3b. The dashed curve is a spatial statistical model built from the $\bar{u}$-forcing patterns. To build the model, we aligned the centroid of the $\bar{u}$-forcing patterns from A3, A5, and C5 at the central latitude of these three regions (28°N, 56°N, and 48°N respectively). We then fit a multiple linear regression model (method in section 2d) in which the zonally averaged δu_{15-151} response was the predictand and the

aligned $\bar{u}$-forcing patterns from A3, A5, and C5 were the predictors. The coefficient in front of the A3 index is negative, consistent with the sign of the associated $\delta\gamma_a$, and the model accounts for slightly more than 80% of the spatial pattern of the zonally averaged response.

To show that RWB accounts for the temporal pattern of the response, particularly the downstream translation of the response, we project δu onto its leading EOF for the domain 42°W to 60°E (Fig. 7). The principal component associated with this leading δu EOF is shown in bold in Fig. 8a and resembles the temporal evolution of the response in geopotential height analyzed in DTP. We developed a multiple linear regression model of the δu principal component (method in section 2d) using time series of γ anomalies corresponding to the A3, A5, and C5 regions in Fig. 5. These time series are shown in Fig. 8b and represent anomalies in the relative frequency of RWB ($\delta\gamma_a$ for the A regions and $\delta\gamma_c$ for the C5 region) for radii of approximately ten degrees of arc length around each region's largest response anomaly. The model is shown as a thin curve in Fig. 8a and accounts for 88% of the δu principal component.

4. Summary and Discussion

We showed how changes in the relative frequencies of anticyclonic and cyclonic RWB explain the transient response of an atmospheric general circulation model to a pattern of winter sea-ice extent forcing. When the CCM3 was forced by North Atlantic sea-ice extent anomalies corresponding to a strong positive NAO, the model developed a localized baroclinic response over the first two weeks. As the baroclinic response intensified, the dominant eddies along 55°N shifted toward lower phase speeds better separated from the critical value equal

to the background zonal wind speed, and a dramatic decrease in anticyclonic RWB ensued. Meanwhile, anticyclonic RWB became more frequent where eddy phase speeds increased toward the background zonal flow along 35°N, and cyclonic RWB became more frequent over eastern Europe. By analyzing how anticyclonic and cyclonic RWB force the background zonal flow, we showed that these changes in RWB relative frequency account for more than 80% of the spatial and temporal pattern of the model's zonal wind response.

Model equilibrium response patterns such as the one examined here are often attributed to, or shown to be in balance with, nonlinear transient eddy feedback. Here, we identify RWB as a specific nonlinear eddy phenomenon whose variability can be affected by an initial baroclinic response and translated into a larger-scale barotropic response. That RWB should be the key element shaping such a response is not surprising given the established linkage between RWB and the NAO. In a previous observational study of reanalysis data, SM8 found that the NAO is highly correlated with RWB over specific regions of the hemisphere. In these regions, RWB generates surface pressure anomalies that project onto the NAO centers of action while generating a pattern of upper tropospheric momentum flux divergence that feeds back onto the background zonal flow so as to maintain the zonal wind pattern characteristic of the NAO spatial pattern. Comparing the SM8 results with the present study, we find close correspondence between the regions where RWB is related to the observed NAO and regions where RWB responses were induced by the sea ice forcing pattern.

We anticipate that the RWB critical line mechanism described here may clarify how the equilibrium response patterns develop in a broad class of boundary forcing experiments, particularly those with response patterns that are NAO-like or are most pronounced near the jet exit regions where RWB is frequent. Previous research has demonstrated the importance

of the location of the forcing relative to the position of the storm track, and the importance of eddy vorticity fluxes in the subsequent evolution of the response. Here, we draw attention to the importance of the position of the critical line relative to the location of the forcing and the resulting modification of the spatiotemporal distribution of RWB. Changes in the background zonal flow or eddy phase speeds resulting from diabatic forcing by sea-ice or SST anomalies can relocate critical lines. The strength of the equilibrium response can then vary considerably depending on the spatial distribution of RWB relative frequency with respect to the relocated critical line. In surf zones where the spectrum of incoming Rossby wave phase speeds and amplitudes is conducive to frequent breaking, critical line modification can have dramatic effects on downstream height and velocity fields as seen in the experiment considered here.

Acknowledgments.

The authors thank C. Deser, R. A. Tomas, and S. Peng for access to their model output, and Christopher Walker for providing the code for the cross-spectral analysis. Comments from three anonymous reviewers helped to improve the manuscript. This research was supported by NSF grant ATM-0612779 and NOAA grant NA06OAR4310149.

REFERENCES

Abatzolglou, J. T. and G. Magnusdottir, 2006: Opposing effects of reflective and nonreflective planetary wave breaking on the NAO. *J. Atmos. Sci.*, **63**, 3448–3457.

Austin, P. C. and J. V. Tu, 2004: Bootstrap methods for developing predictive models. *The American Statistician*, **58**, 131–137.

Chen, G., I. M. Held, and W. A. Robinson, 2007: Sensitivity of the latitude of the surface westerlies to surface friction. *J. Atmos. Sci.*, **64**, 2899–2915.

Chen, G. and P. Zurita-Gotor, 2008: The tropospheric jet response to prescribed zonal forcing in an idealized atmospheric model. *J. Atmos. Sci.*, **65**, 2254–2271.

Deser, C., G. Magnusdottir, R. Saravanan, and A. S. Phillips, 2004: The effects of North Atlantic SST and sea-ice anomalies on the winter circulation in CCM3. Part II: Direct and indirect components of the response. *J. Climate*, **17**, 877–889.

Deser, C., R. A. Tomas, and S. Peng, 2007: The transient atmospheric circulation response to North Atlantic SST and sea ice anomalies. *J. Climate*, **20**, 4751–4767.

Ferreira, D. and C. Frankignoul, 2005: The transient atmospheric response to midlatitude SST anomalies. *J. Climate*, **18**, 1049–1067.

Franzke, C., S. Lee, and S. B. Feldstein, 2004: Is the North Atlantic Oscillation a breaking wave? *J. Atmos. Sci.*, **61**, 145–160.

Hayashi, Y., 1971: A generalized method of resolving disturbances into progressive and retrogressive waves by space Fourier and time cross-spectral analyses. *J. Meteor. Soc. Japan*, **49**, 125–128.

Hoskins, B. J., I. N. James, and G. H. White, 1983: The shape, propagation, and mean-flow interaction of large-scale weather systems. *J. Atmos. Sci.*, **40**, 1595–1612.

Kushnir, Y., , W. A. Robinson, I. Blade, N. M. J. Hall, S. Peng, and R. Sutton, 2002: Atmospheric GCM response to extratropical SST anomalies: Synthesis and evaluation. *J. Climate*, **15**, 2233–2256.

Kushnir, Y. and N.-C. Lau, 1992: The general circulation response to a North Pacific SST anomaly; Dependence on timescale and pattern polarity. *J. Climate*, **5**, 271–283.

Magnusdottir, G., C. Deser, and R. Saravanan, 2004: The effects of North Atlantic SST and sea ice anomalies on the winter circulation in CCM3. Part I: main features and storm track charactersitcs of the response. *J. Climate*, **17**, 857–876.

McIntyre, M. E. and T. N. Palmer, 1983: Breaking planetary waves in the stratosphere. *Nature*, **305**, 593–600.

Peng, S., W. A. Robinson, and M. P. Hoerling, 1997: The modeled atmospheric response to midlatitude sst anomalies and its dependence on background circulation states. *J. Climate*, **10**, 971–987.

Peng, S., W. A. Robinson, and S. Li, 2002: North Atlantic SST forcing of the NAO and relationships with intrinsic hemishperic variability. *Geophys. Res. Lett.*, **29**, doi:10.1029/2001GL014043.

Peng, S., W. A. Robinson, and S. Li, 2003: Mechanisms for the nao response to the North Atlantic SST tripole. *J. Climate*, **16**, 1987–2004.

Randel, W. J. and I. M. Held, 1991: Phase speed spectra of transient eddy fluxes and critical layer absorption. *J. Atmos. Sci.*, **48**, 688–697.

Riviere, G. and I. Orlanski, 2007: Characteristics of the Atlantic storm-track eddy activity and its relation with the North Atlantic Oscillation. *J. Atmos. Sci.*, **64**, 241–266.

Robinson, W. A., 2000: Review of WETS–The workshop on extratropical SST anomalies. *Bull. Amer. Meteor. Soc.*, **81**, 567–577.

Strong, C. and G. Magnusdottir, 2008: Tropospheric Rossby wave breaking and the NAO/NAM. *J. Atmos. Sci.*, **65**, 2861–2876.

Wilks, D. S., 1995: *Statistical methods in the atmospheric sciences*. Academic Press, California.

List of Figures

8 (a) The principal component associated with the zonal wind response EOF in Fig. 7 (bold) and a model constructed from indices representing the response in Rossby wave breaking (thin curve). (b) The Rossby wave breaking response indices used to develop the model in (a). Additional details are given in the text. 27

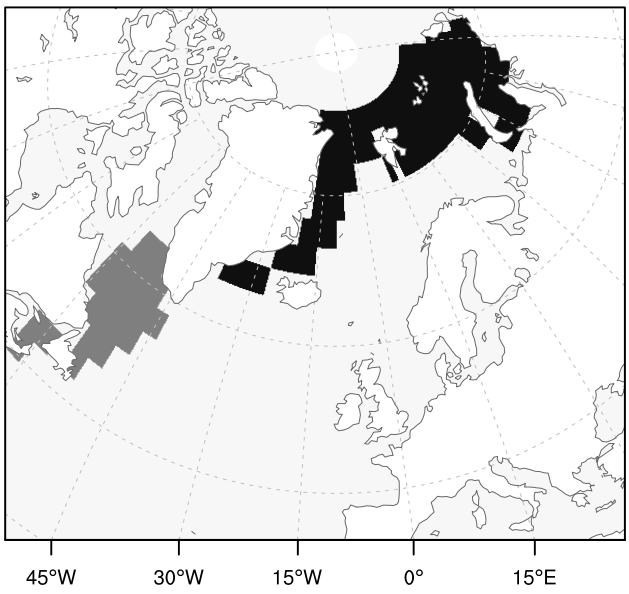

FIG. 1. (a) The sea-ice anomalies for mid-January used in the ICE experiment, where black (gray) shading corresponds to ice removal (addition).

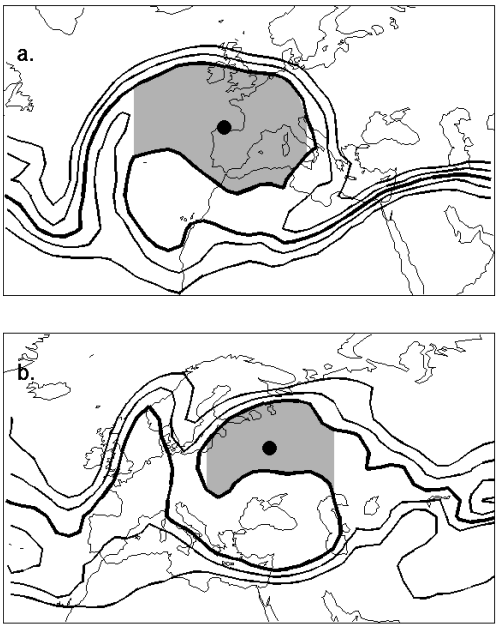

FIG. 2. (a) An example of anticyclonic Rossby wave breaking on 25 December in the second member of the control ensemble. Circumpolar contours of potential vorticity are shown at 1-pvu increments with the 4-pvu contour bold. The poleward tongue associated with the depicted instance of anticyclonically-overturning PV has its area shaded and its centroid marked by a filled circle. (b) Same as (a), but for a case of cyclonic Rossby wave breaking on 08 March in the 28th member of the control ensemble with the 6-pvu contour bold.

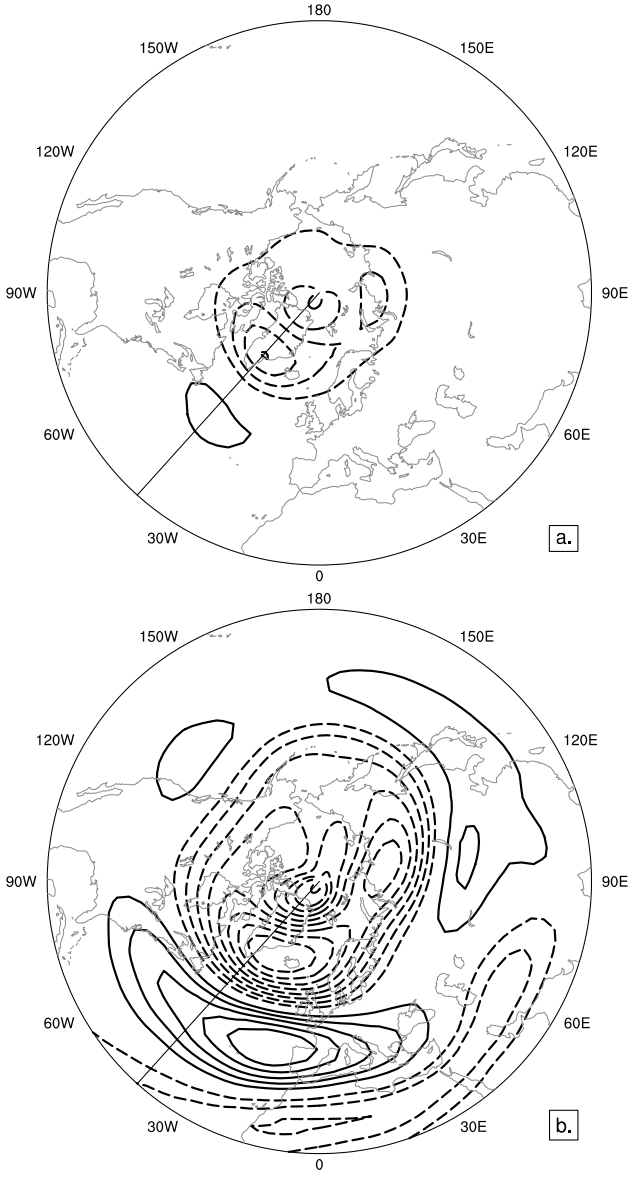

FIG. 3. (a) Response in zonal wind on the 350-K surface averaged over days 1-14 (δu_{1-14}) contoured at 0.1 ms^{-1} with negative values dashed and the zero contour suppressed. (b) Same as (a), except averaged over days 15-151 (δu_{15-151}). The meridian at 42°W is indicated in each panel.

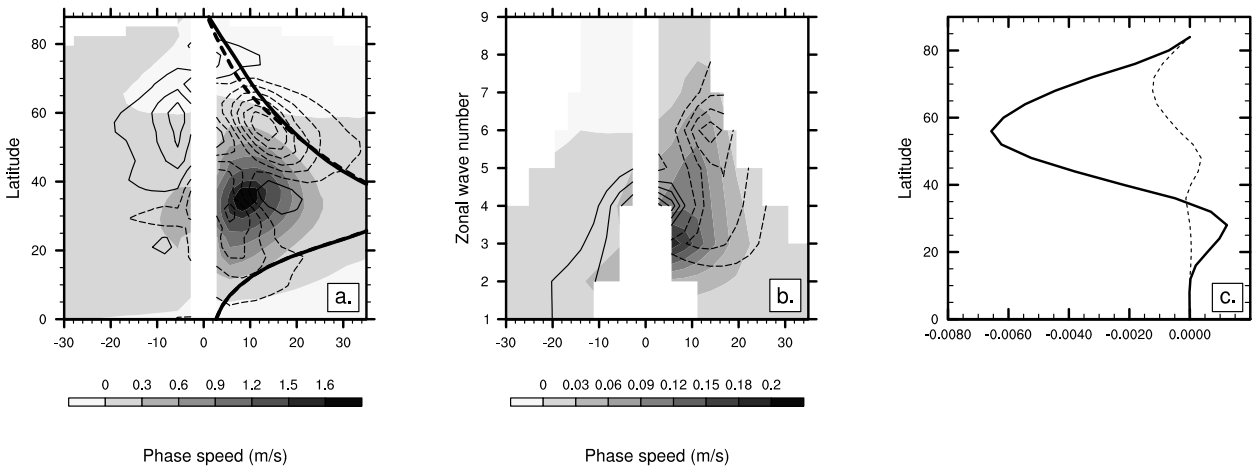

FIG. 4. (a) Eddy momentum flux decomposed by latitude and phase speed for December-January in the control ensemble (shading, $m^2\ s^{-2}$), and the model response for the same field (thin contours at 0.015 $m^2\ s^{-2}$ with negative values dashed and the zero contour suppressed). The bold solid (dashed) curve shows the zonally averaged zonal wind for the control (forced) ensemble. (b) results from 55°N in (a) transformed into zonal wave number / phase speed space with response curves contoured at $5 \times 10^{-3} m^2\ s^{-2}$. (c) Zonally averaged response in the relative frequency of anticyclonic (bold) and cyclonic (dashed) Rossby wave breaking for the entire duration of the experiment.

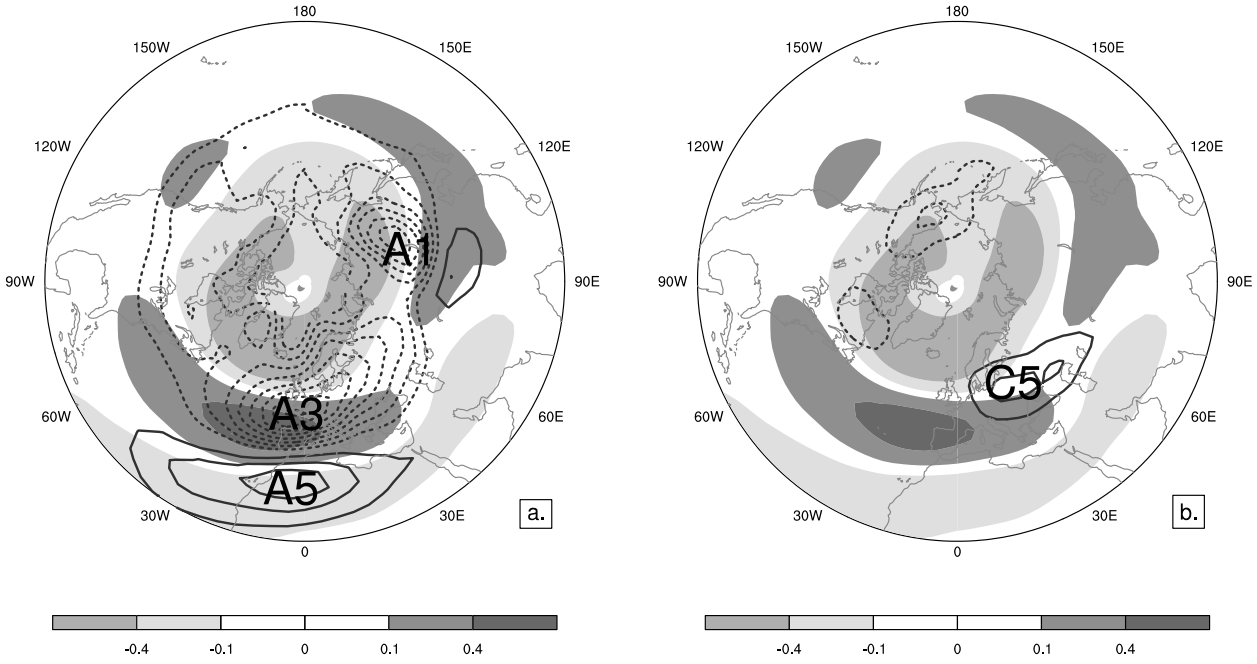

FIG. 5. (a) The response in anticyclonic Rossby wave breaking relative frequency ($\delta\gamma_a$) contoured at 2×10^{-3} with negative values dashed and the zero contour suppressed. Shading shows the basic pattern of the zonal wind response in Fig. 3b. (b) Same as (a), but for cyclonic Rossby wave breaking ($\delta\gamma_c$). The labeled regions are discussed in the text.

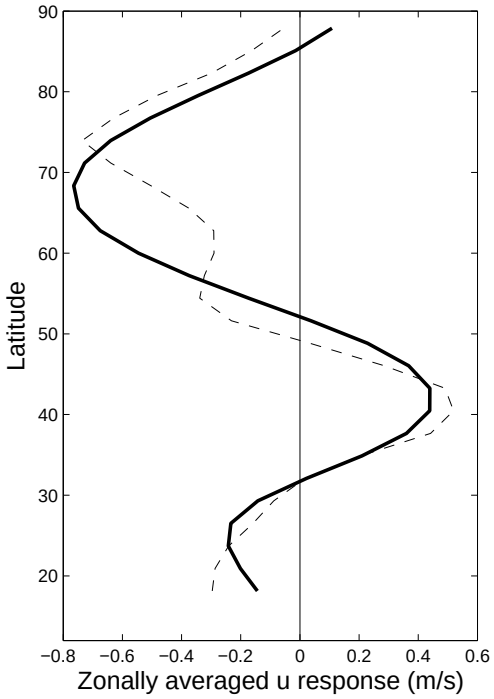

FIG. 6. Zonal average of the zonal wind response from Fig. 3b (bold curve) and a model constructed from the zonal wind forcing patterns of Rossby wave breaking (dashed curve). Additional details on are given in section 3b.

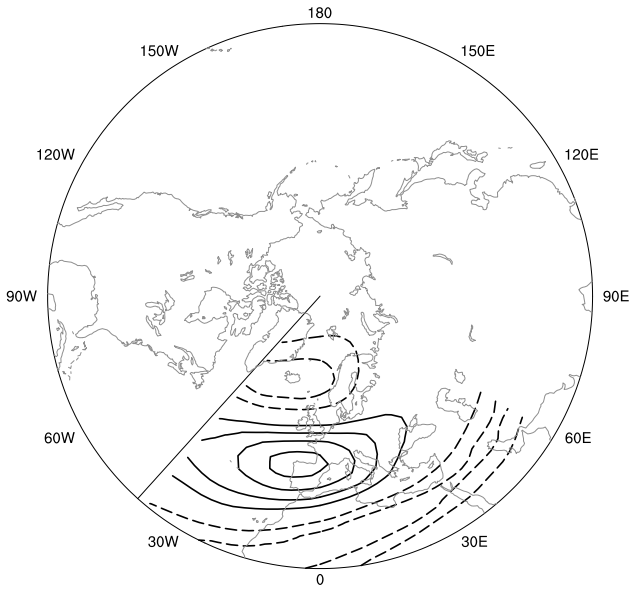

FIG. 7. Leading EOF of the zonal wind response over the domain 42°W to 60°E contoured at 0.02 with negative values dashed and the zero contour suppressed. The meridian at 42°W is indicated to facilitate comparison with Fig. 3.

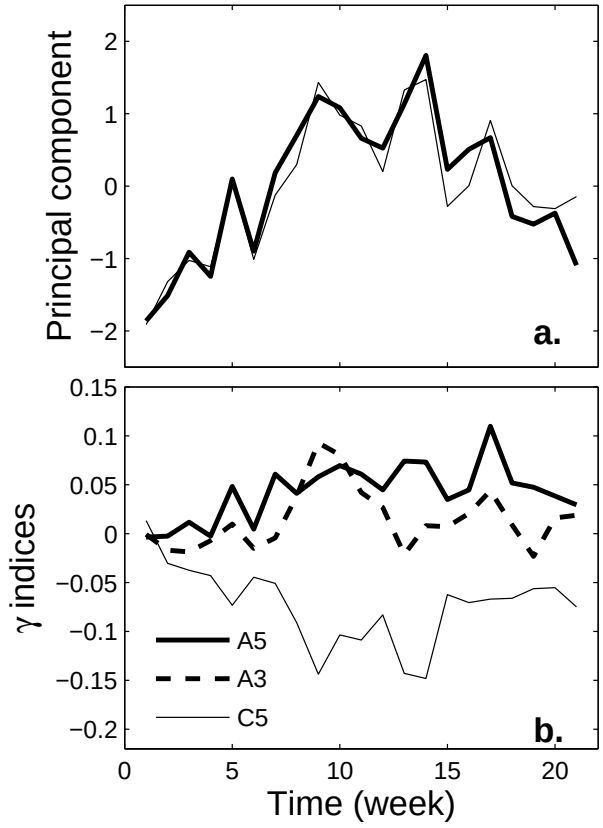

FIG. 8. (a) The principal component associated with the zonal wind response EOF in Fig. 7 (bold) and a model constructed from indices representing the response in Rossby wave breaking (thin curve). (b) The Rossby wave breaking response indices used to develop the model in (a). Additional details are given in the text.